

Dynamic Control of Soft Robots Interacting with the Environment

Cosimo Della Santina*, Robert K. Katzschmann*, Antonio Bicchi, Daniela Rus

Abstract—Despite the emergence of many soft-bodied robotic systems, model-based feedback control has remained an open challenge. This is largely due to the intrinsic difficulties in designing controllers for systems with infinite dimensions. In this paper we propose an alternative formulation of the soft robot dynamics which connects the robot’s behavior with the one of a rigid bodied robot with elasticity in the joints. The matching between the two system is exact under the common hypothesis of Piecewise Constant Curvature. Based on this connection we introduce two control architectures, with the aim of achieving accurate curvature control and Cartesian regulation of the robot’s impedance, respectively. The curvature controller accounts for the natural softness of the system, while the Cartesian controller adapts the impedance of the end effector for interactions with an unstructured environment. This work proposes the first closed loop dynamic controller for a continuous soft robot. The controllers are validated and evaluated on a physical soft robot capable of planar manipulation.

I. INTRODUCTION

Animals move very differently from rigid robots. Animals interact robustly, compliantly, and continuously with the external world through their body’s elasticity, and they perform dynamic tasks efficiently. Inspired by biology, researcher are designing soft robots with elastic bodies [1], for example a soft robotic fish [2], adaptive soft grippers [3], soft worms [4], and soft octopuses [5].

Creating robots with soft bodies promises machines with great motion agility and compliance – such motion requires a *soft robotic brain* to compute the control for the soft body. Soft robotic systems have to robustly manage the intelligence embedded in their complex structure [6] in order to generate reliable and repeatable behaviors. Developing control strategies suited for soft body control has been very challenging. Part of the difficulty is creating an exact mathematical formulation for the soft robotic model, which requires taking into account the infinite dimensionality of the robot’s state space [7].

The theory of infinite state space control is still confined to relatively simple systems, and its applications are still preliminary [8]. The use of learning techniques was considered as a possible alternative in [9], [10]. However, model-based techniques have an important role in achieving

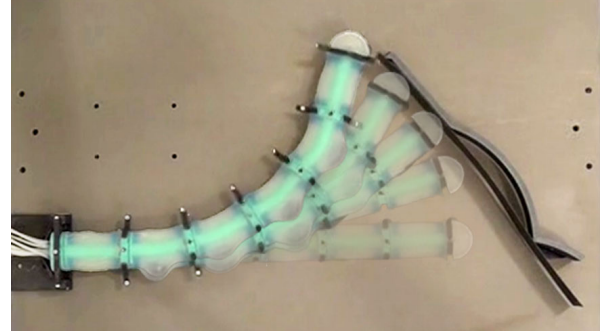


Fig. 1. Dynamically controlled soft robot approaching and then tracing along an environment. The robot has five actuated soft segments and is controlled through a model-based Cartesian feedback controller, one of two control architectures presented in this paper.

higher levels of performance in the control of both artificial and natural systems [11]. This observation drove the development of simplified models capable of describing the robot’s behavior through a finite set of variables. Several works focused on reduced descriptions of the soft robot’s kinematics. Using such models, several quasi-static control strategies were proposed. Finite element methods (FEM) are the most natural way to achieve this goal. FEM-based kinematic models were used to design an algorithm for kinematic inversion [12] and planning [13]. However, a reduced kinematic model most commonly used in soft robotics is the so-called *Piecewise Constant Curvature (PCC)* [14]. Other prior work on modeling and control of soft robots includes modeling biological systems [15], automatically designing the soft robot’s kinematics [16], and developing algorithms for inverse kinematics [17], [18]. The use of purely kinematic strategies for soft robot control, together with heuristically tuned low-level high gain feedback controllers, work well in static situations with sparse contacts with the environment. However, a dynamic model is required for control strategies for dynamic tasks and continuous interactions with the environment. Prior work on dynamic models with finite dimensions includes the Ritz-Galerkin models [19], and the discrete Cosserat models [20]. We are not aware of any prior work that applies these dynamic models to controlling soft robotics. Dynamic models based on the PCC hypothesis were presented in [21] and [22]. In both works, the models are merely used for generating purely feed-forward actuations. To the best of our knowledge, there has been no work on the design of dynamical feedback controllers for continuum soft robots.

In this paper we propose two novel feedback control architectures that were specifically designed for controlling soft

*The authors contributed equally to this work.

R. Katzschmann, and D. Rus are with the Computer Science and Artificial Intelligence Laboratory, Massachusetts Institute of Technology, 32 Vassar St., Cambridge, MA 02139, USA, rkk@csail.mit.edu, rus@csail.mit.edu

C. Della Santina, and A. Bicchi are with Centro E. Piaggio, University of Pisa, Italy, cosimodellasantina@gmail.com

A. Bicchi is also with the Department of Advanced Robotics, Istituto Italiano di Tecnologia, Genoa, Italy, antonio.bicchi@iit.it

robots. The proposed architectures are able to compensate for dynamical forces, while using the intelligence embedded in the soft robotic behavior to stabilize a desired trajectory in the curvature space. The architecture is designed to preserve the natural softness of the robot and adapt to interactions with an environment. The first controller aims to achieve regulation of time-varying curvatures profiles in free space. The second controller is an impedance controller that allows the end effector to control its position in free space and to move along a surface, while staying in contact with that surface. The proposed control scheme is based on an “augmented formulation” linking the soft robot to a classic rigid serial manipulator with a parallel elastic mechanism. Prior tools developed for rigid bodied robots can be used with this formulation [23]–[25].

In this paper we develop the model, design and analyze the control algorithms, and evaluate them in a suite of physical experiments. This work contributes:

- a closed loop dynamic controller for a continuous soft robot capable of dynamically tracking desired curvatures.
- a closed loop dynamic controller for a continuous soft robot capable of moving in Cartesian space and compliantly tracing a surface.
- an “augmented formulation” linking a soft robot to a classic rigid serial manipulator under the PCC hypothesis.
- an experimental validation of the controllers on a planar system.

II. MODEL

In this section, we propose a framework for modeling the dynamics of soft robots, linking it to an equivalent rigid robot constrained through a set of nonlinear integrable constraints. The key property of the model is to define a perfect matching under the hypothesis of piecewise constant curvature, enabling the application of control strategies typically used in rigid robots onto soft robots.

A. Kinematics

In the Piecewise Constant Curvature (PCC) model, the infinite dimensionality of the soft robot’s configuration is resolved by considering the robot’s shape as composed of a fixed number of segments with constant curvature (CC), merged such that the resulting curve is everywhere differentiable. Consider a PCC soft robot composed by n CC segments, and consider a set of reference systems $\{S_0\}, \dots, \{S_n\}$ attached at the ends of each segment. Fig. 2 presents an example of a soft robot composed by four CC segments. Using the constant curvature hypothesis, S_{i-1} and S_i fully define the configuration of the i -th segment. Thus, the robot’s kinematics can be defined by n homogeneous transformations T_0^1, \dots, T_{n-1}^n , which map each reference system to the subsequent one.

In the interest of conciseness, we will consider the planar case. Please refer to [14] for more details about the PCC kinematics in 3D case. Fig. 3 shows the kinematics of a sin-

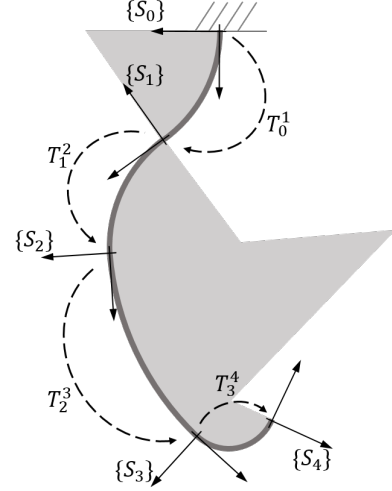


Fig. 2. Example of a Piecewise Constant Curvature robot, composed by four constant curvature elements. $\{S_0\}$ is the robot’s base frame. A reference frame $\{S_i\}$ is connected at the end of each segment. T_{i-1}^i is the homogeneous transformation mapping $\{S_{i-1}\}$ into $\{S_i\}$.

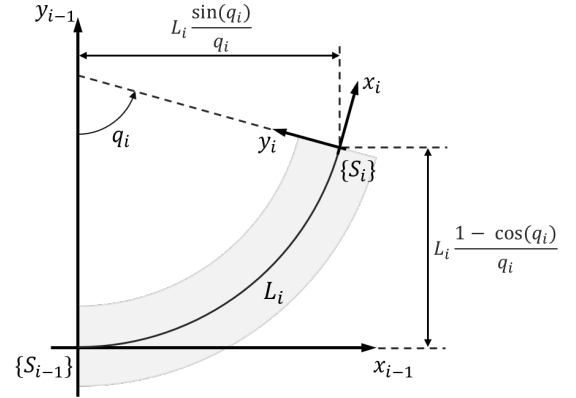


Fig. 3. Kinematic representation of the i -th planar constant curvature segment. Two local frames are placed at the two ends of the segment, $\{S_{i-1}\}$ and $\{S_i\}$ respectively. The length of the segment is L_i , and q_i is the degree of curvature.

gle CC segment. Under the hypothesis of non-extensibility, one variable is sufficient to describe the segment’s configuration. We use the relative rotation between the two reference systems, called the degree of curvature, as the configuration variable. Let us call this variable q_i for the i -th segment. Then, the i -th homogeneous transformation can be derived using geometrical considerations as

$$T_{i-1}^i(q_i) = \begin{bmatrix} \cos(q_i) & -\sin(q_i) & L_i \frac{\sin(q_i)}{q_i} \\ \sin(q_i) & \cos(q_i) & L_i \frac{1 - \cos(q_i)}{q_i} \\ 0 & 0 & 1 \end{bmatrix}, \quad (1)$$

where L_i is the length of a segment.

B. Dynamically-Consistent Augmented Formulation

An equivalent formulation of Eq. (1) in terms of elemental Denavit-Hartenberg (DH) transformations is introduced in

[26]. The framework we propose in this section leverages the intuition that such equivalence implicitly defines a connection between a soft robot and a rigid robot described by the equivalent DH-parametrization. Fig. 4(a) shows an example of robotic structures (an RPR robot) matching a single CC segment. More complex rigid structures matching a generic PCC soft robot can be built by connecting such basic elements.

We will refer to the state space of the equivalent rigid robot as the *augmented state representation* of the PCC soft robot. We call $\xi \in \mathbb{R}^{nm}$ the augmented configuration, where m is the number of joints per CC segment and n is the number of segments. The two configurations are connected through the continuously differentiable map

$$m : \mathbb{R}^n \rightarrow \mathbb{R}^{nm}. \quad (2)$$

The map $\xi = m(q)$ assures that the end points of each CC segment coincide with the corresponding reference points of the rigid robot. Note that from a kinematic point of view, any augment representation satisfying this condition is equivalent. However, as soon as we consider the dynamics of the two robots, another constraint has to be taken into account: the inertial properties of the augmented and the soft robot must be equivalent. We thus ensure that the inertial properties are equivalent by matching the centers of mass of each CC segment by an equivalent point mass in the rigid robot structure. Considering a point mass placed in the middle of the main chord as a suitable approximation of the mass distribution of the CC segment, a dynamically consistent DH parametrization is described in Tab. I. The segment map is

$$m_i(q_i) = \begin{bmatrix} \frac{q_i}{2} \\ L_i \frac{\sin(\frac{q_i}{2})}{q_i} \\ L_i \frac{\sin(\frac{q_i}{2})}{q_i} \\ \frac{q_i}{2} \end{bmatrix}. \quad (3)$$

We show a graphical representation of this robot in Fig. 4(b). A generic PCC continuous soft robot can always be matched to a dynamically consistent rigid robot, built as a sequence of these RPPR elements. We present in Fig. 5 an equivalent rigid formulation for the PCC soft robot of Fig. 2. The robot's configurations are connected by the map

$$m(q) = \begin{bmatrix} m_1(q_1)^T & \dots & m_n(q_n)^T \end{bmatrix}^T. \quad (4)$$

C. Dynamics

Consider the dynamics of the augmented rigid robot

$$B_\xi(\xi)\ddot{\xi} + C_\xi(\xi, \dot{\xi})\dot{\xi} + G_\xi(\xi) = \tau_\xi + J_\xi^T(\xi)f_{\text{ext}}, \quad (5)$$

where $\xi, \dot{\xi}, \ddot{\xi}$ is the robot configuration with its derivatives, B_ξ is the robot's inertia matrix, $C_\xi\dot{\xi}$ collects Coriolis and centrifugal terms, G_ξ takes into account the effect of gravity on the robot. The robot is subject to a set of control inputs

TABLE I
DESCRIPTION OF THE RIGID ROBOT EQUIVALENT TO A SINGLE CC SEGMENT. THE PARAMETERS θ, d, a, α REFER TO THE CLASSIC DH PARAMETRIZATION, WHILE μ REFERS TO THE MASS.

| Link | θ | d | a | α | μ |
|------|-----------------|---------------------------------------|---|------------------|---------|
| 1 | $\frac{q_i}{2}$ | 0 | 0 | $\frac{\pi}{2}$ | 0 |
| 2 | 0 | $L_i \frac{\sin(\frac{q_i}{2})}{q_i}$ | 0 | 0 | μ_i |
| 3 | 0 | $L_i \frac{\sin(\frac{q_i}{2})}{q_i}$ | 0 | $-\frac{\pi}{2}$ | 0 |
| 4 | $\frac{q_i}{2}$ | 0 | 0 | 0 | 0 |

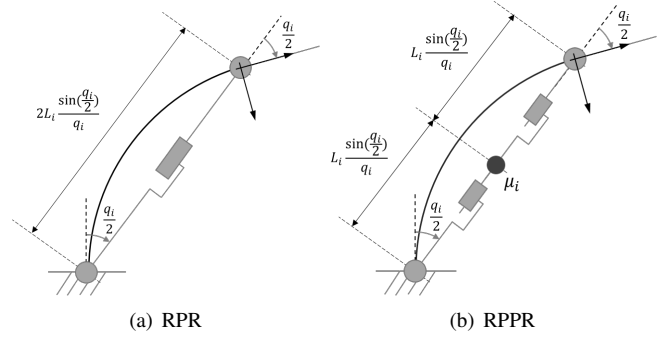


Fig. 4. Two examples of augmented robots kinematically consistent with a planar CC segment. Several of these basic elements can be connected to obtain a kinematically consistent representation of a PCC soft robot. Of the two examples only (b) takes into account the positioning of the mass of the segment, which is here placed in the middle of the chord, i.e. mass concentrated at the two ends of the segment.

τ_ξ , and a set of external wrenches f_{ext} , mapped through the Jacobian J_ξ . To express Eq. (5) on the sub-manifold implicitly identified by $\xi = m(q)$, we evaluate the augmented configuration derivatives $\xi, \dot{\xi}, \ddot{\xi}$, w.r.t. q, \dot{q}, \ddot{q}

$$\begin{cases} \xi = m(q) \\ \dot{\xi} = J_m(q)\dot{q} \\ \ddot{\xi} = \dot{J}_m(q, \dot{q})\dot{q} + J_m(q)\ddot{q} \end{cases} \quad (6)$$

where $J_m(q) : \mathbb{R}^n \rightarrow \mathbb{R}^{nm \times n}$ is the Jacobian of $m(\cdot)$, defined in the usual way as $J_m = \frac{\partial m}{\partial q}$. For example, when $m_i(q_i)$ is defined as in (4), the Jacobian is

$$J_{m,i}(q_i) = \begin{bmatrix} \frac{1}{2} & L_{c,i}(q_i) & L_{c,i}(q_i) & \frac{1}{2} \end{bmatrix}^T \quad (7)$$

where $L_{c,i}(q_i) = L_i \frac{q_i \cos(\frac{q_i}{2}) - 2 \sin(\frac{q_i}{2})}{2 q_i^2}$. By substituting (6) into (5), it follows

$$\begin{aligned} & B_\xi(m(q))(\dot{J}_m(q, \dot{q})\dot{q} + J_m(q)\ddot{q}) \\ & + C_\xi(m(q), J_m(q)\dot{q})J_m(q)\dot{q} + G_\xi(m(q)) \\ & = \tau_\xi + J_\xi^T(m(q))f_{\text{ext}}. \end{aligned} \quad (8)$$

This generalized balance of forces can be projected into the constraints through pre-multiplication with $J_m^T(q)$. This yields the compact dynamics

$$B(q)\ddot{q} + C(q, \dot{q})\dot{q} + G_G(q) = \tau + J^T(q)f_{\text{ext}}, \quad (9)$$

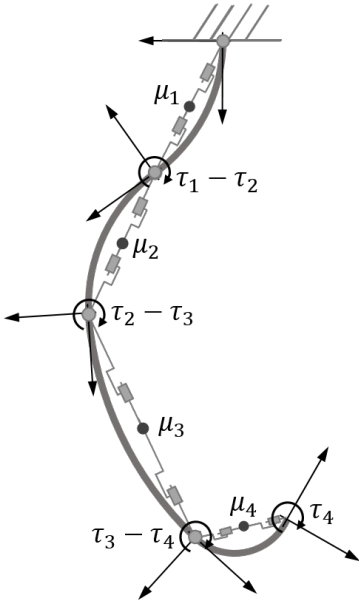


Fig. 5. Example of augmented state representation of a four segment PCC soft robot. Each segment has mass μ_i and it is actuated through a torque τ_i .

where

$$\begin{cases} B(q) &= J_m^T(q) B_\xi(m(q)) J_m(q) \\ C(q, \dot{q}) &= J_m^T(q) B_\xi(m(q)) \dot{J}_m(q, \dot{q}) \\ &\quad + J_m^T(q) C_\xi(m(q), J_m(q) \dot{q}) J_m(q) \\ G_G(q) &= J_m^T(q) G_\xi(m(q)) \\ \tau &= J_m^T(q) \tau_\xi \\ J(q) &= J_\xi(m(q)) J_m(q) \end{cases} \quad (10)$$

Note that the terms in (5) can be efficiently formulated in an iterative form, as discussed in [27]. The soft robotic model (9) inherits this property through (10).

We complete (9) by introducing linear elastic and dissipative terms. The resulting model describing the evolution of the soft robot's degree of curvature q in time is

$$B\ddot{q} + (C + D)\dot{q} + G_G + Kq = \tau + J^T f_{\text{ext}}, \quad (11)$$

where D is the damping and K is the stiffness. Note that the dependencies of q, \dot{q}, \ddot{q} were omitted for the sake of space.

III. CONTROL DESIGN

In the following, we present our proposed controller design for curvature-based dynamic control and Cartesian impedance control with surface following. The uncertainty introduced by the PCC and the hypothesis on the mass distribution must be properly managed by algorithms designed to be robust to model uncertainties. We thus avoid the use of complete feedback cancellations of the robot's dynamics, as well as other kinds of control actions that presented issues with robustness in classical robots, such as pre-multiplications of feedback actions by the inverse of the inertia matrix [25], [28].

A. Curvature Dynamic Control

We propose the following controller for implementing trajectory following in the soft robot's state space

$$\tau = K\bar{q} + D\dot{\bar{q}} + C(q, \dot{q})\ddot{\bar{q}} + B(q)\ddot{\bar{q}} + G_G(q) + I_q \int (\bar{q} - q) \quad (12)$$

where q, \dot{q}, \ddot{q} are the degree of curvature vector and its derivatives. $\bar{q}, \dot{\bar{q}}, \ddot{\bar{q}}$ are the desired evolution and its derivatives expressed in the degree of curvature space. B is the robot's inertia, C is the Coriolis and centrifugal matrix, K and D are respectively the robot's stiffness and damping matrices. The constant I_q is the gain of the integral action.

The resulting form of the closed loop system is

$$\begin{aligned} B(q)(\ddot{q} - \ddot{\bar{q}}) + C(q, \dot{q})(\dot{q} - \dot{\bar{q}}) - J^T(q)f_{\text{ext}} \\ = K(\bar{q} - q) + I_q \int (\bar{q} - q) + D(\dot{\bar{q}} - \dot{q}). \end{aligned} \quad (13)$$

The feed-forward action $K\bar{q} + D\dot{\bar{q}}$ is combined with the physical impedance of the system, generating a natural proportional-derivative (PD) action $K(\bar{q} - q) + D(\dot{\bar{q}} - \dot{q})$. In this way the natural softness of the robot is preserved during possible interactions with an external environment. Please refer to [29] for more details on this. The integral action is included for compensating the mismatches between the real system and the approximated model considered here. Note that I_q is the only parameter that needs to be tuned in the proposed algorithm, since K and D are defined by the physics of the system.

The stability of the closed loop can be proven through arguments similar to the ones in [30]. For the sake of space we will discuss these aspects in more detail in future extensions of this work.

B. Cartesian Impedance Control and Surface Following

A correct regulation of the impedance at the contact point is essential to implement robust and reliable interactions with the environment. Without loss of generality, we will consider in the following as point of contact the soft robot's end effector. We define a local frame $(n_{\parallel}, n_{\perp})$ connected to the end effector, as depicted in Fig. 6. The unit vector n_{\parallel} is chosen to be always tangent to the environment. The

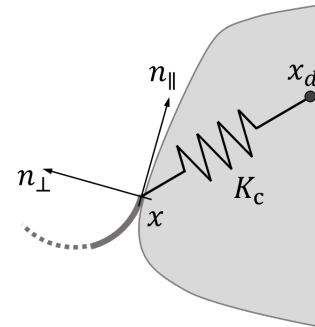


Fig. 6. The goal of the proposed Cartesian impedance controller is to simulate the presence of a spring and a damper connected between the robot's end effector and a point in space x_d . The frame $(n_{\parallel}, n_{\perp})$ defines the tangent and parallel directions to the environment in the contact point.

unit vector n_\perp is such that $n_\parallel^\top n_\perp = 0$, and always points from the inside to the outside of the environment. For the purpose of approaching, contacting, and moving along the environment, we assume the knowledge of the following information:

- the coordinate x_0 of a point included within the environment
- the occurrence of a contact between the end effector and the environment, acquired by `isInContact()`
- parallel n_\parallel and perpendicular n_\perp unit vectors at the contact point, extracted by the methods `readParallelDirection()` and `readPerpendicularDirection()`, respectively
- the final target x_t on the surface of the environment

Note that the occurrence of a contact and the contact direction can be obtained by a motion capture system or an array of force sensors mounted to the end effector.

Leveraging these knowns and the robot's dynamic model, we propose to implement the desired compliant behavior through the following dynamic feedback loop

$$\begin{aligned} \tau = & J^\top(q)(K_c(x_d - x) - D_c J(q)\dot{q}) \\ & + C(q, \dot{q})\dot{q} + G_G(q) + K q \\ & + I_c J^\top(q) n_\parallel \int n_\parallel^\top (x_d - x), \end{aligned} \quad (14)$$

where q, \dot{q} are the degree of curvature vector and its derivative. $J(q)$ is the Jacobian mapping those derivatives into the end effector velocity \dot{x} . x_d is a reference position for the end effector, and x is the current end effector position.

The term $J^\top(q)(K_c(x_d - x) - D_c J(q)\dot{q})$ simulates the presence of a spring and a damper connected between the robot's end effector and x_d . This imposes the desired Cartesian impedance. K_c and D_c are the desired Cartesian stiffness and damping matrices. We choose them to be diagonal in order to implement a full decoupling within the degrees of freedom.

The elements $C(q, \dot{q})\dot{q} + G_G(q) + K q$ cancel the centrifugal, Coriolis, gravitational and elastic force terms. This action is instrumental to obtain the desired decoupling at the end-effector [31].

Finally, we introduce the integral action $I_c J^\top(q) n_\parallel \int n_\parallel^\top (x_d - x)$. Note that we project the error $(x_d - x)$ on the tangent direction n_\parallel . In this way we target the goal of compensating uncertainties introduced by the proposed approximations, obtaining zero error in steady state, while avoiding generating high contact forces.

We specify the values of x_d and n_\parallel on-line through Algorithm 1. Algorithm 1 consists of two phases: approaching and exploring. In the first phase (lines 1-5), a generic point inside the environment x_0 is selected as reference for the impedance controller. No integral action is considered here. When the soft robot makes contact with the environment, the second phase begins (lines 6-10). Here, the desired end effector position is chosen as the final target x_t . A constant displacement $\delta \in \mathbb{R}^+$ in the direction $-n_\perp$ is manually defined to ensure maintenance of contact with the environment. Algorithm 1 terminates when the seminorm of

the error weighted on $n_\parallel n_\parallel^\top$ is under a manually defined threshold. In this way, only the error along the surface is considered.

Algorithm 1 High level control

```

1: while isInContact() == False do                                ▷ Approaching
2:    $n_\parallel \leftarrow [0 \ 0]^\top$ 
3:    $n_\perp \leftarrow [0 \ 0]^\top$ 
4:    $x_d \leftarrow x_0$ 
5: end while
6: while  $\|x - x_d\|_{n_\parallel n_\parallel^\top} > \epsilon$  do                                ▷ Exploring
7:    $n_\parallel \leftarrow \text{readParallelDirection}()$ 
8:    $n_\perp \leftarrow \text{readPerpendicularDirection}()$ 
9:    $x_d \leftarrow x_t - n_\perp \delta$ 
10: end while

```

IV. EXPERIMENTAL RESULTS

In this section, we first describe the experimental setup, followed by the experimental validation of the proposed curvature controller and the Cartesian impedance controller.

A. Experimental setup

The experimental setup used here is a modified version of a soft planar robotic arm used for kinematic motions within confined environments [32] and autonomous object manipulation [33]. The version of the soft robot used here is composed of five bidirectional segments with inflatable cavities. Each segment of the soft arm is 6.3 cm long. The independent pneumatic actuation of the bidirectional arm segments is achieved through an array of 10 pneumatic cylinders. The connection element between each segment is supported vertically by two ball transfers that allow the arm to move with minimal friction on a level plane. A motion tracking system provides real-time measurements of marked points along the inextensible back of the soft arm. A rigid frame holds all the sub-systems together providing reliable hardware experiments without the need for camera recalibration.

B. Identification

The proposed model (11) has several free parameters to be identified: masses μ_i , lengths L_i , stiffnesses k_i , dampings d_i . In addition to the robot's dynamics, we also characterize the behavior of the actuators. The available inputs to our soft robot are the desired placements of the pistons within the cylinders. The placements are expressed in encoder tics, ranging from -1000 to 1000 tics. We model the actuator's dynamics with a second order linear filter $\frac{\alpha_i}{(\gamma_i s + 1)^2}$. α_i and γ_i are two additional variables to be included in the identification. The identification data were collected through three experiments. For each experiment, a step input is injected into all pneumatic cylinders. The amplitudes of the steps were 300, 600, and 900 tics, respectively.

The free parameters L_i and μ_i were directly measured with 0.063 m and 0.034 kg, respectively. We hypothesized the same stiffness and damping for each segment in order

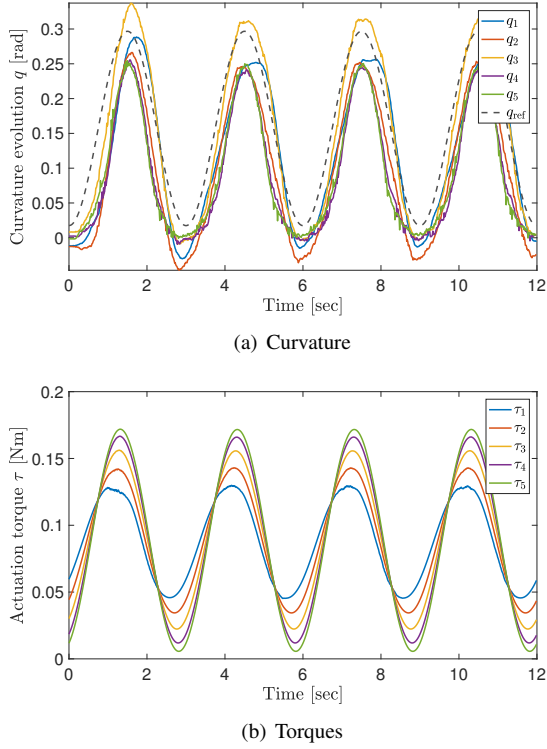


Fig. 7. Evolutions resulting from the application of the dynamic controller (12) to the tracking of a trajectory (15). The integral gain is $I_q = 0 \frac{\text{Nm}}{\text{s}}$. Panel (a) shows the evolution of the degree of curvature q . Panel (b) presents the corresponding actuation torques.

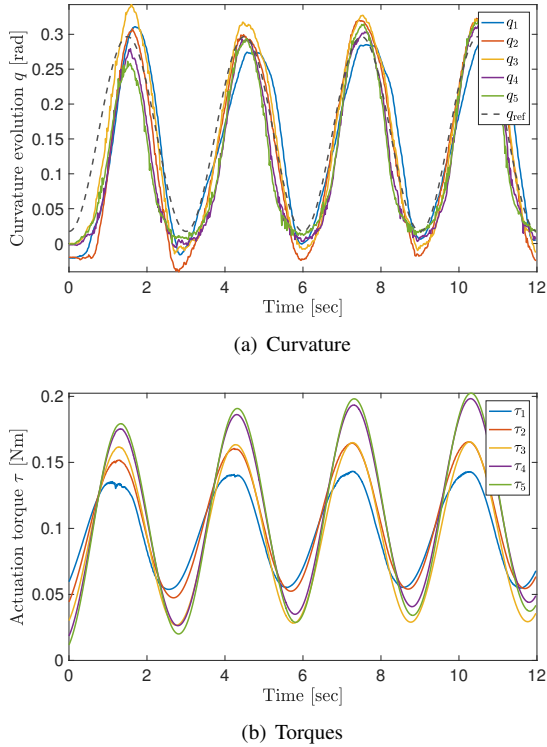


Fig. 8. Evolutions resulting from the application of the dynamic controller (12) to the tracking of a trajectory (15). The integral gain is $I_q = 0.08 \frac{\text{Nm}}{\text{s}}$. Panel (a) shows the evolution of the degree of curvature q . Panel (b) presents the corresponding actuation torques.

to reduce the search space for the identification procedure. We identified the remaining parameters by iteratively fixing δ_i to a value picked from a predefined grid. The remaining seven parameters were identified as the ones minimizing the 2-norm of the error between estimated and measured evolutions. For this regression problem we used the pseudo-inverse to achieve this goal. The best performing set of parameters between all identified sets was chosen. The identified stiffness \hat{k} is 0.56 N m . The damping \hat{d} is 0.1066 N m s . The actuator parameters are $\hat{\alpha} = 10^{-3} [0.16, 0.24, 0.2, 0.25, 0.23] \text{ N}^{-1} \text{ m}^{-1}$ and $\hat{\gamma} = [0.1, 0.25, 0.1, 0.1, 0.1] \text{ s}$.

C. Curvature Control

To test the ability of the proposed curvature controller (12), we consider the problem of tracking the following trajectory in the degree of curvature space

$$\bar{q}_i(t) = \frac{\pi}{20} - \frac{\pi}{24} \cos\left(\frac{2}{3} \pi t\right) \quad \forall i \in \{1, \dots, 5\}. \quad (15)$$

The input to the pistons is generated by filtering τ through

$$\frac{1}{\hat{\alpha}_i} \frac{(\hat{\gamma}_i s + 1)^2}{(5 T s + 1)^2}, \quad (16)$$

where $T = 0.015 \text{ s}$ is the sampling time of the control system.

Fig. 7 presents the evolution of measured degrees of curvature and applied torques, with the integral action set to $I_q = 0 \text{ N m s}^{-1}$. Even without any integral compensation of the model uncertainties, the algorithm is able to produce a stable oscillation close to the commanded one. The correspondent L^2 -norm of the error is 0.1311 rad . Fig. 9 presents the photo sequence of one of the resulting oscillations.

Fig. 8 shows the evolution of the same quantities for $I_q = 0.08 \text{ N m s}^{-1}$. This low gain feedback appears to scarcely modify the torque profile. However this small variation reduces sensibly the tracking error, resulting in a L^2 -norm equal to 0.0965 rad . The error can be further reduced by increasing the gain to 0.3 N m s^{-1} , for which the L^2 -norm is 0.0861 rad .

D. Cartesian Impedance Control and Surface Following

We test the effectiveness of the proposed Cartesian impedance controller and surface following strategy. The robot's goal is to first reach the wall and then slide along it until the desired position is reached. Note that we are not interested in a precise regulation of the contact forces. Instead, the constraint imposed by the environment is purposefully exploited in combination with the decoupled compliance imposed by the control, to naturally generate the interaction forces and guide the end effector toward the desired position.

The input to the pneumatic cylinders is produced by filtering τ in (14) through the filter described in (16). The desired impedance at the end effector is

$$K_c = \begin{bmatrix} 13 & 0 \\ 0 & 13 \end{bmatrix} \text{ N m rad}^{-1} \quad D_c = \begin{bmatrix} 6 & 0 \\ 0 & 6 \end{bmatrix} \text{ N m s rad}^{-1}. \quad (17)$$

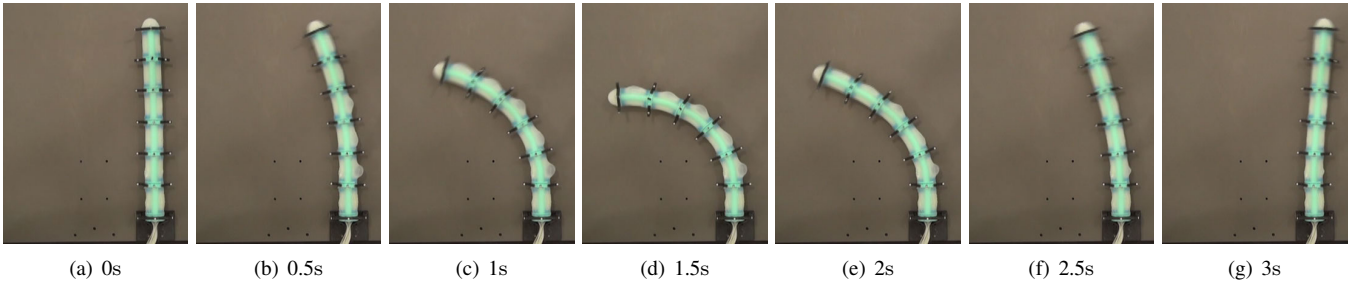


Fig. 9. The photo sequence shows the soft robot controlled along the reference trajectory (15) by the proposed curvature controller (12). No integral action is used here, i.e. $I_q = 0 \frac{\text{Nm}}{\text{s}}$. Note that the bottom segment is not actuated and constrained in its vertical position through a mechanical stop.

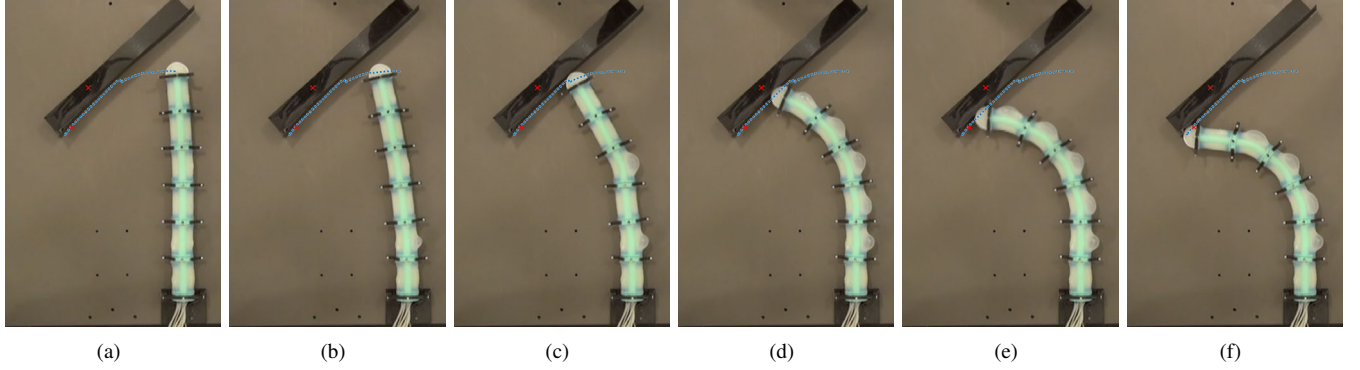


Fig. 10. Photo sequence of the soft robot controlled through the proposed Cartesian impedance controller (14). We report superimposed the two reference positions commanded by Algorithm 1 (red crosses) and the trajectory of the end effector (blue dashed line). Panels (a-c) show the first phase of the algorithm: the robot's tip is attracted toward the environment by a virtual spring connected to a reference point inside the surface. Panels (d-f) illustrate the second phase of the algorithm: the robot traces along the surface toward the desired end position. Note that the bottom segment is not actuated and constrained in its vertical position through a mechanical stop.

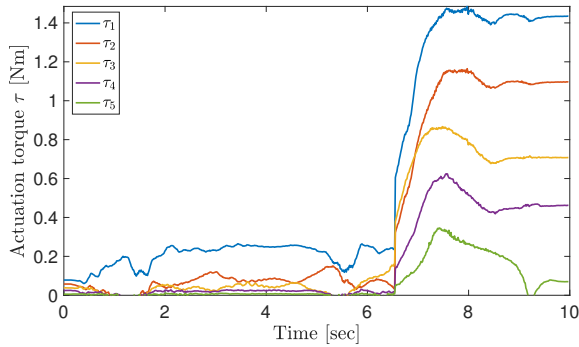


Fig. 11. Actuation torques commanded by the proposed Cartesian impedance controller (14) while executing the Algorithm 1. The contact detection happens at 6.5 s.

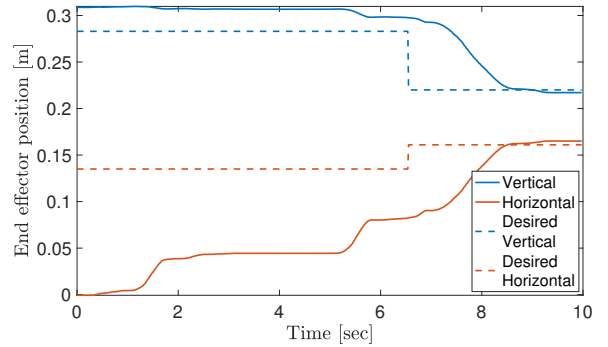


Fig. 12. End effector's evolution in Cartesian space resulting by the application of the proposed Cartesian impedance controller (14) and Algorithm 1. The contact detection happens at 6.5 s.

The integral gain is $I_c = 1.9 \text{ N m rad}^{-1} \text{ s}^{-1}$.

As described in Algorithm 1, the experiment is divided in two phases. In the first one, the end effector of the soft robot is attracted toward a point within the environment ($x_0 = [0.283, 0.135] \text{ m}$), which is manually defined.

After contact is established, it triggers the execution of the second phase. The end-effector is now pulled towards a new target ($x_d = [0.220, 0.160] \text{ m}$) while staying in contact. The distance to the wall is maintained with $\delta = 0.05 \text{ m}$. The values of n_\perp and n_\parallel are considered known.

For one example experiment, the commanded actuation

torques are shown in Fig. 11. The evolution of the end effector in Cartesian space is shown in Fig. 12, while the correspondent photo sequence is shown in Fig. 10.

V. CONCLUSION

In this paper we present two new algorithms that achieve dynamic control of soft robots and enable interactions between soft robots and their environment. Both algorithms leverage on the idea of connecting the soft robot to an equivalent augmented rigid robot, in such a way that the matching is exact in the common hypothesis of constant

curvature, and under the introduced hypothesis on the mass distribution. Classic tools in robotic control are used to develop robust feedback control strategies able to compensate for any model mismatch. We implement the control algorithms on a planar multi-link soft robotic manipulator and demonstrate curvature control and surface following using our strategy.

The control algorithm presented in this paper has been evaluated in the context of exploring a two-dimensional surface using a soft planar robot manipulator. However, the potential for this work is much broader. The control algorithm is general and has the potential to enable a wide range of dynamic tasks, ranging from exploring three dimensional spaces through contact, learning the geometry of the world, picking up delicate objects, moving heavy objects and enabling dynamic interactions with the world.

ACKNOWLEDGMENT

This research was conducted in the Distributed Robotics Laboratory at MIT with support from the National Science Foundation (grant NSF 1117178, NSF IIS1226883, NSF CCF1138967) and with support from SOMA (grant 645599) — project of the European Commission’s Horizon 2020 research program. We are grateful for this support.

REFERENCES

- [1] D. Rus and M. T. Tolley, “Design, fabrication and control of soft robots,” *Nature*, vol. 521, no. 7553, pp. 467–475, 2015.
- [2] R. K. Katzschmann, A. D. Marchese, and D. Rus, “Hydraulic Autonomous Soft Robotic Fish for 3D Swimming,” in *2014 International Symposium on Experimental Robotics (ISER 2014)*, vol. 109, no. 1122374, Marrakech, Morocco, 2014, pp. 405–420.
- [3] R. Deimel and O. Brock, “A novel type of compliant and underactuated robotic hand for dexterous grasping,” *The International Journal of Robotics Research*, vol. 35, no. 1-3, pp. 161–185, 2016.
- [4] S. Seok, C. D. Onal, K.-J. Cho, R. J. Wood, D. Rus, and S. Kim, “Meshworm: a peristaltic soft robot with antagonistic nickel titanium coil actuators,” *IEEE/ASME Transactions on mechatronics*, vol. 18, no. 5, pp. 1485–1497, 2013.
- [5] C. Laschi, M. Cianchetti, B. Mazzolai, L. Margheri, M. Follador, and P. Dario, “Soft robot arm inspired by the octopus,” *Advanced Robotics*, vol. 26, no. 7, pp. 709–727, 2012.
- [6] R. Pfeifer, M. Lungarella, and F. Iida, “The challenges ahead for bio-inspired soft robotics,” *Communications of the ACM*, vol. 55, no. 11, pp. 76–87, 2012.
- [7] D. Trivedi, A. Lotfi, and C. D. Rahn, “Geometrically exact models for soft robotic manipulators,” *IEEE Transactions on Robotics*, vol. 24, no. 4, pp. 773–780, 2008.
- [8] Z.-H. Luo, B.-Z. Guo, and Ö. Morgül, *Stability and stabilization of infinite dimensional systems with applications*. Springer Science & Business Media, 2012.
- [9] D. Braganza, D. M. Dawson, I. D. Walker, and N. Nath, “A neural network controller for continuum robots,” *IEEE transactions on robotics*, vol. 23, no. 6, pp. 1270–1277, 2007.
- [10] M. Giorelli, F. Renda, G. Ferri, and C. Laschi, “A feed-forward neural network learning the inverse kinetics of a soft cable-driven manipulator moving in three-dimensional space,” in *Intelligent Robots and Systems (IROS), 2013 IEEE/RSJ International Conference on*. IEEE, 2013, pp. 5033–5039.
- [11] M. Kawato, “Internal models for motor control and trajectory planning,” *Current opinion in neurobiology*, vol. 9, no. 6, pp. 718–727, 1999.
- [12] Z. Zhang, J. Dequidt, A. Kruszewski, F. Largilliere, and C. Duriez, “Kinematic modeling and observer based control of soft robot using real-time finite element method,” in *Intelligent Robots and Systems (IROS), 2016 IEEE/RSJ International Conference on*. IEEE, 2016, pp. 5509–5514.
- [13] A. Lismonde, V. Sonnevile, and O. Bröls, “Trajectory planning of soft link robots with improved intrinsic safety,” *IFAC-PapersOnLine*, vol. 50, no. 1, pp. 6016–6021, 2017.
- [14] R. J. Webster III and B. A. Jones, “Design and kinematic modeling of constant curvature continuum robots: A review,” *The International Journal of Robotics Research*, vol. 29, no. 13, pp. 1661–1683, 2010.
- [15] S. Sareh, J. Rossiter, A. Conn, K. Drescher, and R. E. Goldstein, “Swimming like algae: biomimetic soft artificial cilia,” *Journal of the Royal Society Interface*, p. rsif20120666, 2012.
- [16] G. Runge and A. Raatz, “A framework for the automated design and modelling of soft robotic systems,” *CIRP Annals-Manufacturing Technology*, 2017.
- [17] A. D. Marchese and D. Rus, “Design, kinematics, and control of a soft spatial fluidic elastomer manipulator,” *The International Journal of Robotics Research*, vol. 35, no. 7, pp. 840–869, 2016.
- [18] H. Wang, B. Yang, Y. Liu, W. Chen, X. Liang, and R. Pfeifer, “Visual servoing of soft robot manipulator in constrained environments with an adaptive controller,” *IEEE/ASME Transactions on Mechatronics*, vol. 22, no. 1, pp. 41–50, 2017.
- [19] S. H. Sadati, S. E. Naghibi, I. D. Walker, K. Althoefer, and T. Nanayakkara, “Control space reduction and real-time accurate modeling of continuum manipulators using ritz and ritz-galerkin methods,” *IEEE Robotics and Automation Letters*, vol. 3, no. 1, pp. 328–335, 2018.
- [20] F. Renda, F. Boyer, J. Dias, and L. Seneviratne, “Discrete cosserat approach for multi-section soft robots dynamics,” *arXiv preprint arXiv:1702.03660*, 2017.
- [21] V. Falkenhahn, A. Hildebrandt, R. Neumann, and O. Sawodny, “Model-based feedforward position control of constant curvature continuum robots using feedback linearization,” in *Robotics and Automation (ICRA), 2015 IEEE International Conference on*. IEEE, 2015, pp. 762–767.
- [22] A. D. Marchese, R. Tedrake, and D. Rus, “Dynamics and trajectory optimization for a soft spatial fluidic elastomer manipulator,” *The International Journal of Robotics Research*, vol. 35, no. 8, pp. 1000–1019, 2016.
- [23] A. Albu-Schaffer, O. Eiberger, M. Grebenstein, S. Haddadin, C. Ott, T. Wimbock, S. Wolf, and G. Hirzinger, “Soft robotics,” *IEEE Robotics & Automation Magazine*, vol. 15, no. 3, 2008.
- [24] C. Ott, *Cartesian impedance control of redundant and flexible-joint robots*. Springer, 2008.
- [25] L. Sciavicco and B. Siciliano, *Modelling and control of robot manipulators*. Springer Science & Business Media, 2012.
- [26] M. W. Hannan and I. D. Walker, “Kinematics and the implementation of an elephant’s trunk manipulator and other continuum style robots,” *Journal of Field Robotics*, vol. 20, no. 2, pp. 45–63, 2003.
- [27] R. Featherstone, *Rigid body dynamics algorithms*. Springer, 2014. [Online]. Available: <http://www.springerlink.com/index/10.1007/978-0-387-74315-8>
- [28] J. Nakanishi, R. Cory, M. Mistry, J. Peters, and S. Schaal, “Operational space control: A theoretical and empirical comparison,” *The International Journal of Robotics Research*, vol. 27, no. 6, pp. 737–757, 2008.
- [29] C. Della Santina, M. Bianchi, G. Grioli, F. Angelini, M. Catalano, M. Garabini, and A. Bicchi, “Controlling soft robots: balancing feedback and feedforward elements,” *IEEE Robotics & Automation Magazine*, vol. 24, no. 3, pp. 75–83, 2017.
- [30] B. Paden and R. Panja, “Globally asymptotically stable ‘pd+’ controller for robot manipulators,” *International Journal of Control*, vol. 47, no. 6, pp. 1697–1712, 1988.
- [31] O. Khatib, “A unified approach for motion and force control of robot manipulators: The operational space formulation,” *IEEE Journal on Robotics and Automation*, vol. 3, no. 1, pp. 43–53, 1987.
- [32] A. D. Marchese, R. K. Katzschmann, and D. Rus, “Whole Arm Planning for a Soft and Highly Compliant 2D Robotic Manipulator,” in *Intelligent Robots and Systems (IROS), 2014 IEEE/RSJ International Conference on*. IEEE, 2014, pp. 554–560.
- [33] R. K. Katzschmann, A. D. Marchese, and D. Rus, “Autonomous Object Manipulation Using a Soft Planar Grasping Manipulator,” *Soft Robotics*, vol. 2, no. 4, pp. 155–164, dec 2015. [Online]. Available: <http://online.liebertpub.com/doi/10.1089/soro.2015.0013>